Published by Nigerian Society of Physical Sciences. Hosted by FLAYOO Publishing House LTD

Proceedings of the Nigerian Society of Physical Sciences

Journal Homepage: https://flayoophl.com/journals/index.php/pnspsc

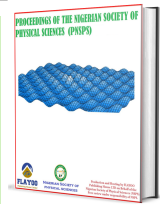

Investigation of the geomagnetic storms' impact on low-latitude ionosphere: case studies of October 2003 and March 2015 events

Hammed Adeniyi Lawal[a,b,*], Isreal Leke Elijah[a], Edwin Beshel Ayabie[a], Yusuf Ayoola Bello[a], Joseph O. Alao[a], Innocent E. Davidson[b]

[a]*Department of Physics, Air Force Institute of Technology, Nigerian Air Force Base, Nigeria*
[b]*Department of Electrical, Electronic and Computer Engineering, French-South African Institute of Technology (F'SATI), Cape Peninsula University of Science and Technology, Cape Town, South Africa*

A B S T R A C T

Geomagnetic storms can significantly impact the Earth's ionosphere, which is crucial for communication and navigation, particularly at low latitudes. This study examines the effects of two major geomagnetic storms on the low-latitude ionosphere that occurred during October 2003 and March 2015. In the analysis of the two events, data from NASA Space Physics data resources, Omni web, were analysed. Our analysis of the electron density, temperature, and ion composition data reveals significant disturbances in the ionosphere during both storms. The October 2003 storm caused a decrease in electron density and an increase in temperature, while the March 2015 storm had a more moderate impact. Our findings underscore the significance of understanding geomagnetic storms' effects on the low-latitude ionosphere, aiding in mitigating their impact on radio communication, navigation, and satellite operations. This study contributes to our understanding of geomagnetic storms' effects on the ionosphere and provides valuable insights for future research and applications.

Keywords: Geomagnetic storms, Low latitude ionosphere, Ionospheric composition.

DOI:10.61298/pnspsc.2025.2.155

1. INTRODUCTION

Geomagnetic storm can be defined as an interval of time when a sufficiently intense and long-lasting interplanetary convection electric field leads, through a substantial energization in the magnetosphere-ionosphere system, to an intensified ring current sufficiently strong enough to exceed some key threshold of the quantifying storm time *Dst* index [1–4]. Magnetospheric storms and substorms influence the ionosphere by altering the critical frequency and altitude of the F region during disturbances. The critical frequency first increases before the storm (substorm) active phase, then decreases during the active phase, and increases again after this phase. On the contrary, the *F* region altitude increases during the active phase and decreases after this phase [5]. A geomagnetic storm is a complex process: its various features act at different heights. Space weather events, particularly intense geomagnetic storms pose significant challenges to our technological infrastructure and satellite-dependent systems revolving through the ionosphere [6].

*Corresponding Author Tel. No.: +234-905-8448-329.
e-mail: hadelawal@yahoo.co.uk, lawalh@cput.ac.za (Hammed Adeniyi Lawal)

```
# prompt: open this data with pandas /content/goess_part_flux_PSM.csv

import pandas as pd
import numpy as np


df = pd.read_excel('/content/omni_hro2_1min (1).xlsx')

# Replace specific values with NaN
df = df.replace([99999.9, 999.99, 9999999.0, 9999.99,99.99],0)

print(df.columns)
print(df.head)

import matplotlib.pyplot as plt

# Assuming 'time' is your index, if not, set it using df.set_index('time')
df.plot(y=['BX, nT (GSE)', 'BY, nT (GSE)', 'BZ, nT (GSE)'], x="Date (DD/MM/YYYY)",
        figsize=(10, 6),  # Adjust figure size as needed
        title='Magnetic Field Components',
        xlabel='Time',
        ylabel='Magnetic Field (nT)')

plt.grid(True)  # Add a grid for better readability
plt.legend()  # Show legend to identify each component
plt.tight_layout()  # Adjust layout for better spacing
plt.show()
```

Figure 1. Sample implementation of codes.

In the *F2* layer the midlatitude effect is basically an ionospheric response to storm-induced changes in the neutral atmosphere, which are primarily a consequence of a strong Joule heating in the auroral thermosphere. At lower heights the role of ionization and photochemical processes increases due to shorter electron lifetimes. At the base of the *F1* layer (160–170 km) the storm effect is almost absent. At *E*-region maximum a complex action of several factors results in a slight decrease of *foF2*, even though below and above, the electron density increases.

Farther down, in the lower ionosphere, a strong increase of the electron density is observed as a consequence of a very strong enhancement of particle precipitation. In the neutral upper middle atmosphere, the effects of enhanced precipitation weaken with decreasing altitude and become insignificant and/or absent in the stratosphere. The effect of geomagnetic storms reappear in the lower atmosphere but as an effect of different morphology and origin, there at least three altitudinal regions of distinctly different geomagnetic storm-related processes responsible for observed effects:

1. F2 layer, where the ionospheric effect is basically a response to storm-time changes of the neutral thermosphere caused primarily by Joule heating.
2. The lower ionosphere and upper middle atmosphere, where the effects are caused by storm-related injections and precipitation of energetic particles of magnetospheric origin.
3. The lower atmosphere, where the effect has different morphology as well as mechanisms, which are possibly related to changes in galactic cosmic ray flux and atmospheric electricity.

The effects of a geomagnetic storm are generally strongest in the auroral zone, their amplitude weakens toward middle latitudes, some of them disappear at low latitudes, but some of them reappear or strengthen near the geomagnetic equator, namely effects in the *F* region [7].

The study drawing inference from Refs. [8–11] is aimed at examining the effects of the October 2003 and March 2015 geomagnetic storms on the ionospheric parameters, such as electron density, total electron content and ionospheric currents, at low latitudes.

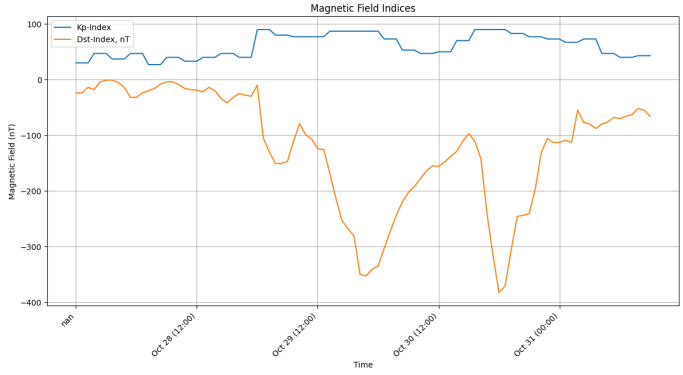

Figure 2. Kp-index (blue) and dst-index (Orange) of Oct 28-31, 2003.

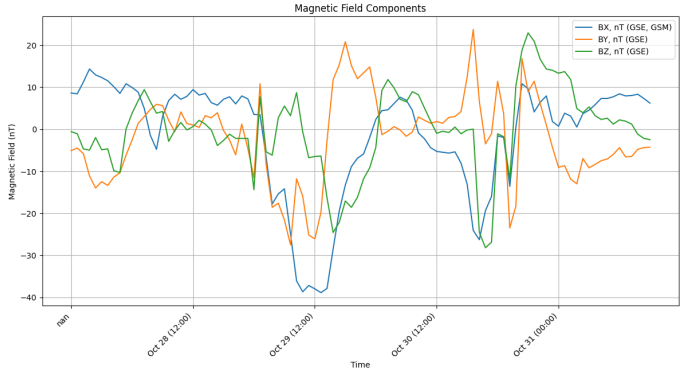

Figure 3. Magnetic field (Bx (blue), By (orange) and Bz (green)) of Oct 28-31, 2003.

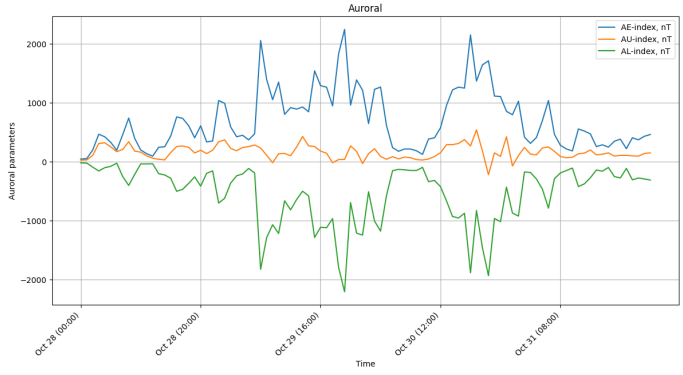

Figure 4. Auroral (AE-index (blue), AU-index (orange) and AL-index (green)) of Oct 28-31, 2003.

2. MATERIALS AND METHODS

This research utilized various solar and geomagnetic datasets, including:

i. Solar storm data (Dst-index, Kp-index)
ii. Auroral indices (AE, AU, AL)
iii. Solar activity indices (R, F10.7)
iv. Interplanetary magnetic field data (Bx, By, Bz)
v. Flow pressure data (nPa).

Drawing inference from Ref. [12] these datasets were obtained from NASA's Omniweb (https://omniweb.gsfc.nasa.gov/

Table 1. Geomagnetic storm details of specified time frame.

Date (Time)		Oct 28 (10:00)	Oct 29 (23:00)	Oct 30 (22:00)	Oct 31 (00:00)
Kp-Index		47	87	90	83
Dst-Index (nT)		-32	-350	-383	-307
Magnetic Field	Bx, GSE (nT)	9.9	-6.9	-1.6	-13.6
	By, GSE (nT)	-2.6	12	11.4	-23.5
	Bz, GSE (nT)	3.8	-16.2	-1.1	-11.9
Auroral	AE-index	162	-31	89	-73
	AU-index	-37	-1243	-1015	-869
	AL-index	199	1212	1104	795
Solar activity parameters	R (Sunspots No.)	270.9	275.4	267.6	245.2
	F10.7_Solar index	247	250	250	239
	Flow pressure, nPa	1.61	0	0	0

Table 2. Data from the IRI model.

Date (Time)		Oct 28 (10:00)	Oct 29 (23:00)	Oct 30 (22:00)	Oct 31 (00:00)
Electron density	Ne (cm^{-3})	1.14e6	1.13e6	1.12e6	1.11e6
	Ne/NmF2	0.971	0.972	0.973	0.975
Temperature	Tn (k)	984	972	982	1007
	Ti (k)	1000	995	1000	1011
	Te (k)	1665	1659	1654	1647
Ion percentage (%) & Ion density	O+	98.8 & 1.13e7	98.8 & 1.11e7	98.8 & 1.10e7	98.8 & 1.09e7
	N+	1.1 & 1.25e5	1.1 & 1.24e5	1.1 & 1.23e5	1.1 & 1.22e5
	H+	0	0	0	0
	He+	0	0	0	0
	O_2+	0	0	0	0
	NO+	0	0	0	0
TEC ($1\times10^{16}m^{-2}$)	Cluster	-1	-1	-1	-1
	TEC	28.2	28	27.7	27.5
	t (%)	64	64	64	64

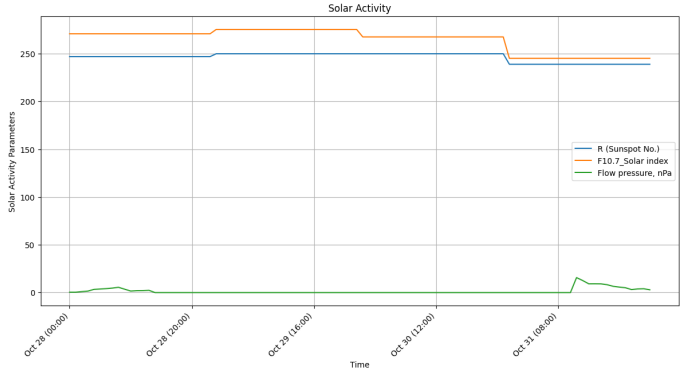

Figure 5. Solar parameters (R (Sunspot No.) (blue), F10.7 Solar index (orange) and Flow pressure, nPa (green)) of Oct 28-31, 2003.

Table 3. Data from superDARN model.

Date (Time)	Potential (kV)		Convection velocity (m/s)	Resultant $\sqrt{By^2 + B_z^2}$ (nT)
	North Hemisphere	South Hemisphere		
Oct 28 (10:00)	18	21	1000	4
Oct 29 (23:00)	78	83	1000	20
Oct 30 (22:00)	59	59	1000	11
Oct 31 (00:00)	60	81	1000	26

form/dx1.html) and the World Data Center (WDC) for Geomagnetism, Kyoto Japan (https://wdc.kugi.kyoto-u.ac.jp/), for the periods of October 28-31, 2003, and March 16-18, 2015.

Our methodology consisted of the following steps:

i. Data collection: We retrieved the required datasets from NASA's Omniweb and the WDC.

ii. Data preprocessing: We used Python libraries, including Pandas and NumPy, to clean and preprocess the data.

iii. Data analysis: We employed visualization libraries, such as Matplotlib and Seaborn, to generate plots and analyze the data.

iv. Modeling: We utilized the International Reference Ionosphere (IRI) model version 2020 (https://kauai.ccmc.gsfc.nasa.gov/instantrun/iri/) to obtain electron density, temperature, total electron content, and ion composition in the low-latitude ionosphere. Additionally, we used the Su-

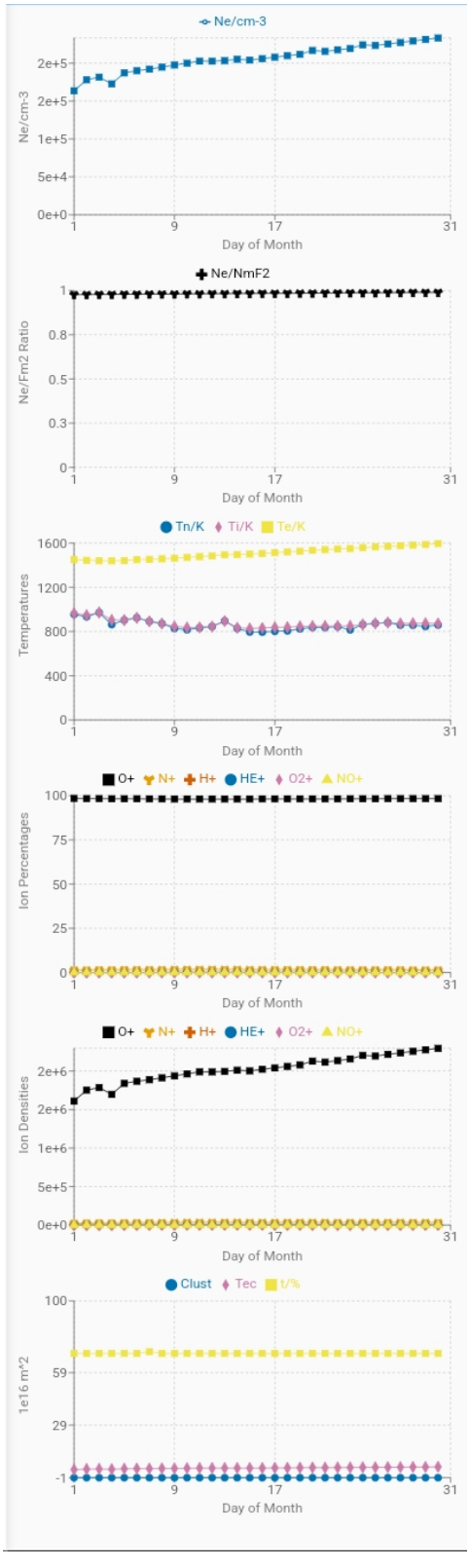

Figure 6. Snapshot of IRI model showing the temperature (Tn, Ti, and Te), the electron density (Ne/cm^{-3} and Ne/NmF2), the ion densities and percentages of O, N, H, HE, O^2 and NO, and the total electron count (TEC) of March 2003

perDARN convection model (https://kauai.ccmc.gsfc.nasa.gov/instantrun/superdarn/).

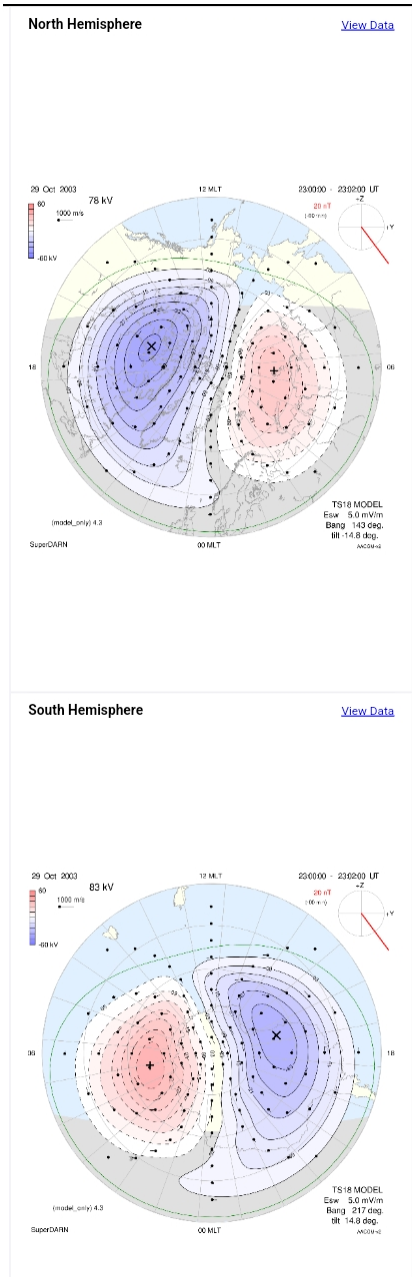

Figure 7. Snapshot of North and South hemisphere SuperDARN convection model of Oct 28 and 29 (10:00-10:02 and 23:00 – 23:02) 2003

By following these steps, we ensured a clear and reproducible methodology for our research.

3. RESULTS AND DISCUSSIONS

3.1. OCTOBER 2003

We considered the time period from each day (Oct 28-31), which had the most storm intensity, which are: Oct 28 (10:00), Oct 29 (23:00), Oct 30 (22:00) and Oct 31 (00:00). From Figures 2 to 5 above, concentrating on the time period of the most storm intensity, we retrieved the data below:

Also, using the known information that the low-latitude ionosphere typically refers to the region of the ionosphere that lies between 30°S and 30°N magnetic latitude and in terms of altitude, it is divided into 3 main sub-region, which are; D-region of

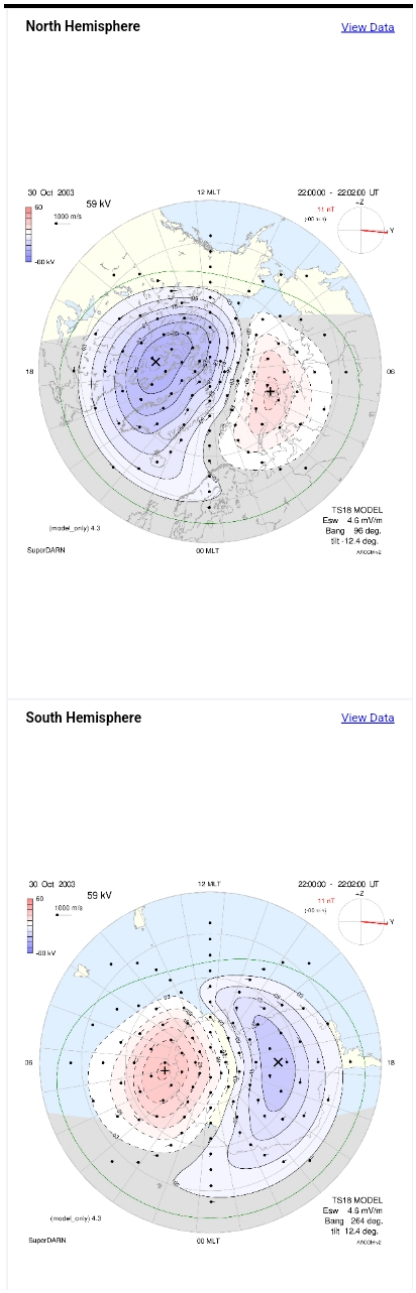

Figure 8. Snapshot of North and South hemisphere SuperDARN convection model of Oct 30 and 31 (22:00-22:02 and 00:00-00:02) 2003.

about 50-100km altitude, E-region of about 100-150km altitude and F-region of about 150-600km altitude. For this research, we focused specifically on the F-region. We made use of the stated Magnetic latitude and the altitude of the F-region to get the models of *Figure 6 above,* then concentrating on the time frame of the most storm intensity, we retrieved the data in Table 2.

Furthermore, we made use of the magnetic field data (By and Bz) to get the model of Figures 7 and 8, then concentrating on the time period of the most storm intensity, we retrieved the data in Table 3.

From Table 1, it was observed that Oct 30 (22:00) had the most intense storm activity – dst-index of -383nT and Kp-index of 90, followed by Oct 29 (23:00) – dst-index of -350nT and Kp-index

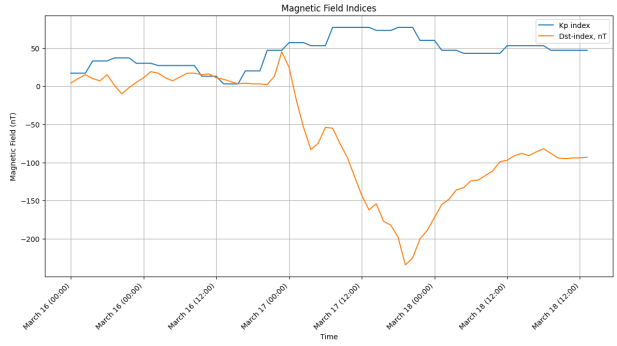

Figure 9. Kp-index (blue) and dst-index (Orange) of March 16-18, 2015.

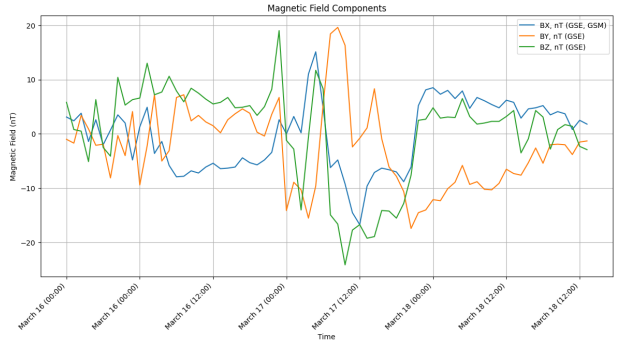

Figure 10. Magnetic field (Bx (blue), By (orange) and Bz (green)) of March 16-18, 2015.

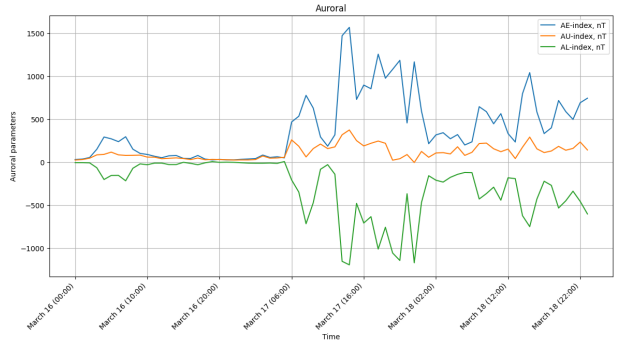

Figure 11. Auroral (AE-index (blue), AU-index (orange) and AL-index (green)) of March 16-18, 2015.

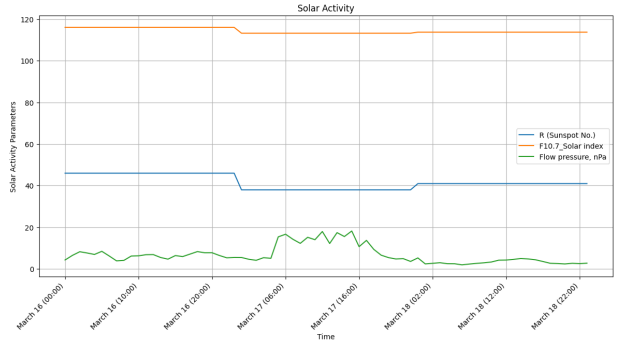

Figure 12. Solar parameters (R (Sunspot No.) (blue), F10.7_Solar index (orange) and flow pressure, nPa (green)) of March 16-18, 2015.

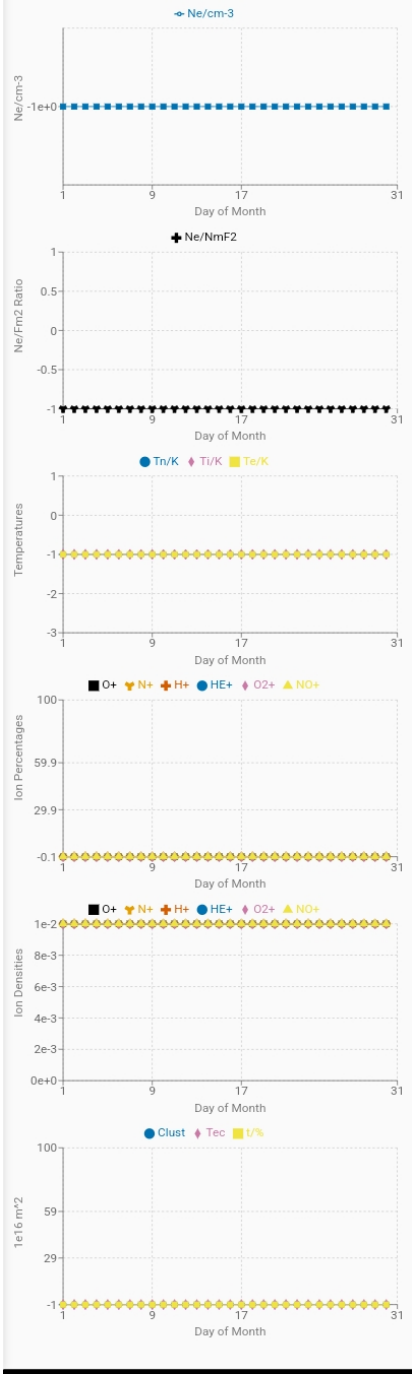

Figure 13. Snapshot of IRI model showing the temperature (Tn, Ti, and Te), the electron density (Ne/cm^{-3} and Ne/NmF2), the ion densities and percentages of O, N, H, HE, O^2 and NO, and the total electron count (TEC) of Oct 2015.

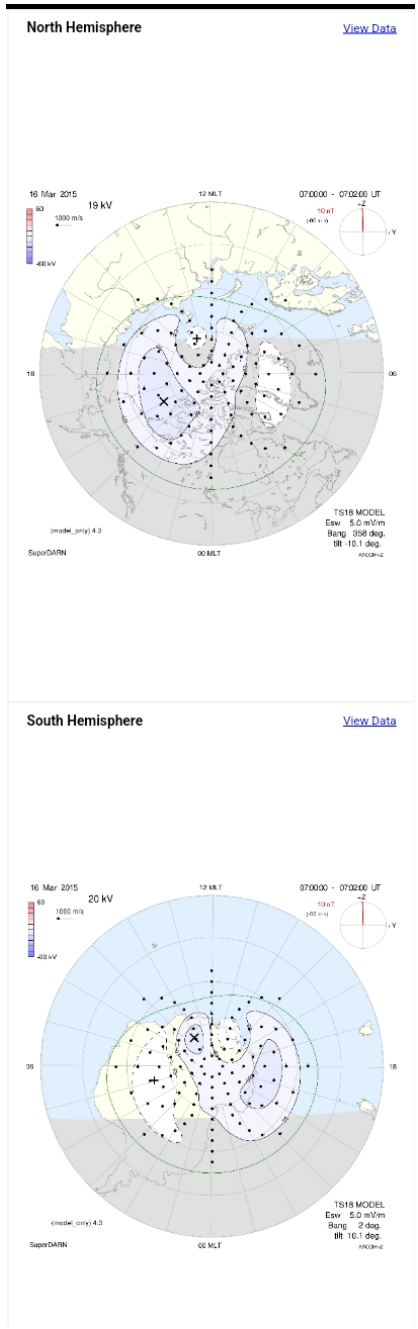

Figure 14. Snapshot of North and South hemisphere SuperDARN convection model of March 16 and 17 (07:00-07:02 and 22:00 – 22:02) 2015.

of 87, then Oct 31 (00:00) – dst-index of -307nT and Kp-index of 83 and finally Oct 28 (10:00) – dst-index of -32nT and Kp-index of 47 . For the Auroral, Oct 29 (23:00) has a value of -31 for AE-index, -1243 for AL-index and 1212 for AL-index, followed by Oct 30 (22:00) which has a value of 89 for AE-index, -1015 for AL-index and 1104 for AL-index, then Oct 31 (00:00) which has a value of -73 for AE-index, -869 for AL-index and 795 for AL-index and finally Oct 28 (10:00) which has a value of 162 for AE-index, -37 for AL-index and 199 for AL-index. Also Oct 29 (23:00) has a value of 275.4 for R (Sunspots No.), 250 for F10.7_Solar index and 0 for Flow pressure, nPa, followed by Oct 30 (22:00) which has a value of 267.6 for R (Sunspots No.), 250

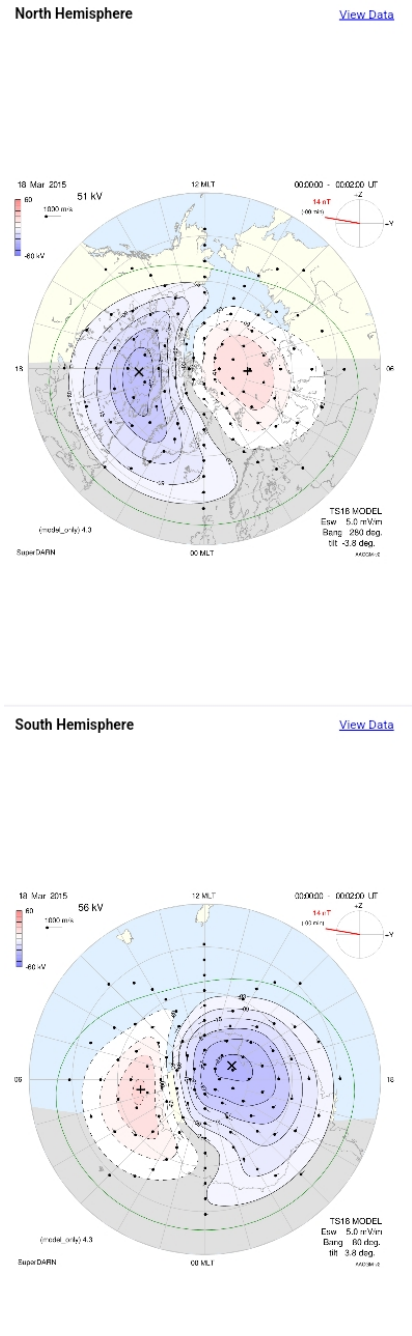

Figure 15. Snapshot of North and South hemisphere SuperDARN convection model of March 18 (00:00-00:02) 2015.

for F10.7_Solar index and 0 for Flow pressure, nPa, then Oct 28 (10:00) which has a value of 270.9 for R (Sunspots No.), 247 for F10.7_Solar index and 1.61 for Flow pressure, nPa and finally Oct 31 (00:00) which has a value of 245.2 for R (Sunspots No.), 239 for F10.7_Solar index and 0 for Flow pressure, nPa.

Also, we observed from Table 2, that the electron density (Ne), was on a steady decrease across Oct 28 (10:00) – Oct 31 (00:00) while Ne/NmF2 (NmF2 is the F2 peak density) was increasing; the temperature (Tn) was on a steady increase, Ti (ion temperature) was fluctuating and and Te (electron temperature) was decreasing; the ion with most prominent percentage in the ionosphere across this time frame was O+ (98.8%), follow by N+ (1.1%), and then the H+, He+, O_2+ and NO+ are all 0); O+ was the ion with the greatest density and decreased across Oct 28 (10:00) – Oct 31 (00:00), N+ had the second highest density, it was also decreasing across Oct 28 (10:00) – Oct 31 (00:00), the other ions densities were all 0; the electron cluster was constant (-1), total electron count (TEC) was on a steady decrease across the time frame with its percentage above F peak (t) being constant 64 across the stated timeframe.

Table 4. Geomagnetic storm details of the specified time frame.

Date (Time)		March 16 (07:00)	March 17 (22:00)	March 18 (00:00)
Kp-Index		37	77	60
Dst-Index (nT)		-10	-234	-200
Magnetic Field	Bx, GSE (nT)	3.5	-8.8	2.5
	By, GSE (nT)	-0.3	-10.6	-1.5
	Bz, GSE (nT)	10.4	-12.8	-2.3
Auroral	AE-index	79	89	125
	AU-index	-217	-368	-470
	AL-index	296	457	595
Solar activity parameters	R (Sunspots No.)	116	113.2	113.7
	F10.7_Solar index	46	38	41
	Flow pressure, nPa	3.9	4.98	5.32

Furthermore, we observed from Table 3, that the convection velocity was constant (1000m/s), the potential (kV) for Oct 29 (23:00) was highest for North hemisphere (78) and South hemisphere (83), it also is the second highest resultant (By and Bz) of 20nT, followed by Oct 31 (00:00) – 60 for the North and 81 for the South, with highest resultant value of 26, then Oct 30 (22:00) – constant of 59 for both North and South hemisphere with a resultant value of 11 and finally Oct 28 (10:00) – 19 for the North and 21 for the South, resultant value of 4.

We discovered that the most intense storm activity occurred on October 30 (22:00) with a Dst-index of -383nT and Kp-index of 90, the auroral indices showed significant variations, the electron density decreased steadily, while Ne/NmF2 increased, the dominant ion was O+ (98.8%), followed by N+ (1.1%) and that the convection velocity was constant at 1000 m/s.

3.2. MARCH 2015

We considered the time from each day (March 16-18), which had the most storm intensity, which are; March 16 (07:00), March 17 (22:00) and March 18 (00:00). From Figures 9 - 12, concentrating on the time of the most storm intensity, we retrieved the data in Table 4.

Also, using the known information that the low-latitude iono-

Table 5. Data from the IRI model.

Date (Time)		March 16 (07:00)	March 17 (22:00)	March 18 (00:00)
Electron density	Ne (cm^{-3})	-1	-1	-1
	Ne/NmF2	-1	-1	-1
Temperature	Tn (k)	-1	-1	-1
	Ti (k)	-1	-1	-1
	Te (k)	-1	-1	-1
Ion percentage (%) & Ion density	O+	-0.1 & 1e-2	-0.1 & 1e-2	-0.1 & 1e-2
	N+	-0.1 & 1e-2	-0.1 & 1e-2	-0.1 & 1e-2
	H+	-0.1 & 1e-2	-0.1 & 1e-2	-0.1 & 1e-2
	He+	-0.1 & 1e-2	-0.1 & 1e-2	-0.1 & 1e-2
	O_2+	-0.1 & 1e-2	-0.1 & 1e-2	-0.1 & 1e-2
	NO+	-0.1 & 1e-2	-0.1 & 1e-2	-0.1 & 1e-2
TEC ($1\times10^{16}m^{-2}$)	Cluster	-1	-1	-1
	TEC	-1	-1	-1
	t (%)	-1	-1	-1

Table 6. Data from superDARN model.

Date (Time)	Potential (kV)		Convection velocity (m/s)	Resultant $\sqrt{By^2 + B_z^2}$ (nT)
	North Hemisphere	South Hemisphere		
March 16 (07:00)	18	21	1000	4
March 17 (22:00)	78	83	1000	20
March 18 (00:00)	59	59	1000	11

sphere typically refers to the region of the ionosphere that lies between 30°S and 30°N magnetic latitude and in terms of altitude, it is divided into 3 main sub-region, which are; D-region of about 50-100km altitude, E-region of about 100-150 km altitude and F-region of about 150-600km altitude. For this research, we focused specifically on the F-region. We made use of the stated Magnetic latitude and the altitude of the F-region to get the models of Figure 13 then concentrating on the time frame of the most storm intensity, we retrieved the data in Table 5.

Furthermore, we made use of the magnetic field data (By and Bz) to get the model of Figures 14 – 15, then concentrating on the time period of the most storm intensity, we were retrieved the data in Table 6.

From Table 4, it was observed that March 17 (22:00) had the most intense storm activity with dst-index of -234nT and Kp-index of 77, followed by March 18 (00:00) with dst-index of -200nT and Kp-index of 60 and then the March 16 (07:00) with dst-index of -10nT and Kp-index of 37. For the Auroral, March 16 (07:00) has a value of 79 for AE-index, -217 for AL-index and 296 for AL-index, followed by March 17 (22:00) which has a value of 89 for AE-index, -368 for AL-index and 457 for AL-index and finally March 18 (00:00) which has a value of 125 for AE-index, -470 for AL-index and 595 for AL-index. Also March 16 (07:00) has a value of 116 for R (Sunspots No.), 46 for F10.7_Solar index and 3.9 for Flow pressure, nPa, followed by March 17 (22:00) which has a value of 113.2 for R (Sunspots No.), 38 for F10.7_Solar index and 4.98 for Flow pressure, nPa and finally March 18 (00:00) which has a value of 113.7 for R (Sunspots No.), 41 for F10.7_Solar index and 5.32 for Flow pressure, nPa.

Also, we observed from Table 5, that the electron density (Ne and Ne/NmF2 – NmF2 is the F2 peak density), the temperature (Tn, Ti – ion temperature and Te – electron temperature), the electron cluster, total electron count (TEC), the percentage above F peak (t), the ion percentage were all a constant of -1, the ion density was also a constant of 1e-2 across March 16 (07:00) – March 18 (00:00).

Furthermore, we observed from Table 6, that the Potential (kV) of March 17 (22:00) was the highest value for both the North hemisphere (78) and the South hemisphere (83), followed by March 18 (00:00) which has a constant value of 59 for both North and South hemisphere and finally March 16 (07:00) with va 18 for the North hemisphere and 21 for the Sputh, the resultant (By and Bz) of March 17 (22:00) as seen from the table was the highest (20) followed by that of March 18 (00:00) – 11 and finally March 16 (07:00) – 4. The Convection velocity was constant (1000m/s).

We discovered that the most intense storm activity occurred on March 17 (22:00) with a Dst-index of -234nT and Kp-index of 77, the auroral indices showed significant variations, with the highest values occurring on March 18 (00:00), the ionospheric parameters remained relatively constant over the three days and that the potential was highest on March 17 (22:00) for both the North and South hemispheres.

Our analysis of the October 2003 and March 2015 geomagnetic storms revealed distinct characteristics and impacts on the low-latitude ionosphere. The October 2003 storm exhibited the most intense activity, with a Dst index of -383 nT and a Kp index of 90. In contrast, the March 2015 storm had a Dst index of -234 nT and a Kp index of 77. Both storms displayed significant changes in auroral activity, as indicated by the AE, AL, and AU indices, and were characterized by high sunspot numbers and F10.7 solar index values, signifying intense solar activity. The October 2003 storm also showed exceptionally high flow pres-

sure values.

Our investigation of ionospheric parameters revealed substantial changes in electron density, temperature, and composition during both storms. Specifically, the electron density decreased steadily during the October 2003 storm, accompanied by a temperature increase and a shift in ion composition, with O+ becoming the dominant ion. These findings demonstrate that geomagnetic storms can profoundly impact the low-latitude ionosphere, causing changes in electron density, temperature, and composition. Our results have important implications for understanding the effects of geomagnetic storms on the low-latitude ionosphere and for refining predictive models of space weather..

4. CONCLUSION

In summary, our study demonstrates the significant impact of geomagnetic storms on the low-latitude ionosphere. The October 2003 and March 2015 storms were particularly intense, causing changes in electron density, temperature, and composition. Future research should further investigate the effects of geomagnetic storms on the ionosphere and the mechanisms driving these variations. Additionally, improved space weather models are needed to enhance prediction and mitigation strategies.

DATA AVAILABILITY

The solar and geomagnetic datasets (Solar storm, Auroral indices, Solar activity indices, Interplanetary magnetic field data and Flow pressure) is available at https://omniweb.gsfc.nasa.gov/form/dx1.html and https://wdc.kugi.kyoto-u.ac.jp/. The International Reference Ionosphere (IRI) model version 2020 is available at https://kauai.ccmc.gsfc.nasa.gov/instantrun/iri/. The SuperDARN convection model is available at https://kauai.ccmc.gsfc.nasa.gov/instantrun/superdarn/.

References

[1] S. I. Akasofu, "A review of the current understanding in the study of geomagnetic storms", Int. J. Earth Sci. Geophys **4** (2018) 18. https://doi.org/10.35840/2631-5033%2F1818.

[2] W. D. Gonzalez, J. A. Joselyn, Y. Kamide, H. W. Kroehl, G. Rostoker, B. T. Tsurutani & V. M. Vasyliunas, "What is a geomagnetic storm?", Journal of Geophysical Research: Space Physics **99** (1994) 5771. https://doi.org/10.1029/93JA02867.

[3] V. Habyarimana, J. B. Habarulema & T. Dugassa, "Analysis of ionospheric storm-time effects over the East African sector during the 17 March 2013 and 2015 geomagnetic storms", Earth, Planets and Space **75** (2023) 58. https://doi.org/10.1186/s40623-023-01812-9.

[4] Y. Kamide, W. Baumjohann, I. A. Daglis, W. D. Gonzalez, M. Grande, J. A. Joselyn & V. M. Vasyliunas, "Current understanding of magnetic storms: storm-substorm relationships", Journal of Geophysical Research: Space Physics **103** (1998) 17705. https://doi.org/10.1029/98JA01426.

[5] C. M. Anoruo, B. Rabiu, D. Okoh, F. N. Okeke & K. C. Okpala, "Irregularities in the African ionosphere associated with total electron content anomalies observed during high solar activity levels", Frontiers in Astronomy and Space Sciences **9** (2022) 947473. https://doi.org/10.3389/fspas.2022.947473.

[6] D. M. Oliveira, E. Zesta & D. Nandy, "The 10 October 2024 geomagnetic storm may have caused the premature reentry of a Starlink satellite", Frontiers in Astronomy and Space Sciences **11** (2025) 1522139.https://doi.org/10.3389/fspas.2024.1522139.

[7] A. D. Danilov & J. Lastovicka, "Effects of geomagnetic storms on the ionosphere and atmosphere", International Journal of Geomagnetism and Aeronomy **2** (2001) 209. https://citeseerx.ist.psu.edu/document?repid=rep1&type=pdf&doi=04ad6b0986495fc998f1039a9a5a5ef30afa0bad.

[8] M. Chakraborty, S. Kumar, B. K. De & A. Guha, "Effects of geomagnetic storm on low latitude ionospheric total electron content: A case study from Indian sector", Journal of Earth System Science **124** (2015) 1115. https://doi.org/10.1007/s12040-015-0588-3.

[9] S. Ramsingh, S. Sripathi, S. Sreekumar, S. Banola, K. Emperumal, P. Tiwari & B. S. Kumar, "Low-latitude ionosphere response to super geomagnetic storm of 17/18 March 2015: Results from a chain of ground-based observations over Indian sector", Journal of Geophysical Research: Space Physics **120** (2015) 10. https://doi.org/10.1002/2015JA021509.

[10] W. Zhang, X. Zhao, S. Jin & J. Li, "Ionospheric disturbances following the March 2015 geomagnetic storm from GPS observations in China", Geodesy and Geodynamics **9** (2018) 288. https://doi.org/10.1016/j.geog.2018.02.001.

[11] D. V. Blagoveshchenskii, "Effect of geomagnetic storms (substorms) on the ionosphere: A review", Geomagnetism and Aeronomy **53** (2013) 275. https://doi.org/10.1134/S0016793213030031.

[12] D. R. Themens, S. Elvidge, A. McCaffrey, P. Jayachandran, A. Coster, R. H. Varney & B. Reid, "The high latitude ionospheric response to the major May 2024 geomagnetic storm", A synoptic view. Geophysical Research Letters **51** (2024) e2024GL111677. https://doi.org/10.1029/2024GL111677.